Astron. Astrophys. 363, 926–932 (2000)

ASTRONOMY
AND
ASTROPHYSICS

0.6 resolution images at 11 and 20 μm of the active galactic nucleus in NGC 1068*

D. Alloin[1], **E. Pantin**[2], **P.O. Lagage**[2], **and G.L. Granato**[3]

[1] European Southern Observatory, Casilla 19001, Santiago, Chile
[2] DSM/DAPNIA/Service d'Astrophysique, CEA/Saclay, 91191 Gif-sur-Yvette, France
[3] Osservatorio Astronomico di Padova, 35122 Padova, Italy

Received 8 August 2000 / Accepted 8 August 2000

Abstract. We present diffraction-limited IR images at 11.2 and 20.5 μm of the central $6'' \times 6''$ region in NGC 1068, collected with the CAMIRAS instrument mounted at the f/36 IR focus of the CFHT/Hawaii 3.6m telescope and at the f/35 IR focus of the ESO/La Silla 3.6m telescope, respectively. After deconvolution, the achieved resolution ($0.6''$) reveals a prominent central core emitting about 95% of the total flux at these wavelengths, as well as extended emission, to the South-West (PA = 210°) and to the North-East (PA = 35°), broken into patchy components which are particularly conspicuous at 20.5 μm and can be isolated as individual clouds. The central core shows an East-West FWHM of $0.6''$ (hence unresolved) and a North-South FWHM of $0.9''$ corresponding to a resolved full size extension of $\approx$ 100 pc. Such an elongated shape is in agreement with model predictions of a dusty/molecular torus surrounding the central engine in NGC 1068, observed under an inclination angl of around 65°. Considering that the core at 11.2 and 20.5 μm is coincident with the core also seen at 2.2, 3.5 and 4.8 μm and that this features the location of the central engine (also the radio source S1), the extended mid-IR emission is found to follow closely the radio jet–like structure in both the North-East and South-West quadrants. In the North-East quadrant, we observe that the mid-IR emission arises predominantly on the eastern side of the ionizing cone defined by the HST NLR [OIII]–emitting clouds and is still quite prominent at the wide base of the so-called Northeast radio lobe, $4''$ away from the central engine. A detailed comparison of the extended mid-IR emission with model predictions requires that future AGN modeling includes both a molecular/dusty torus and a distribution of material away from the equatorial plane of the torus, i.e. in and around the NLR.

Key words: galaxies: individual: NGC 1068 – galaxies: Seyfert – galaxies: nuclei – galaxies: active – infrared: galaxies

Send offprint requests to: D. Alloin (dalloin@eso.org)

* Based on observations collected at the ESO/La Silla 3.6m telescope, Proposal 62.P-0445, and at the CFHT/Hawaii 3.6m telescope.

1. Introduction

The current unification scheme for Active Galactic Nuclei (herefater AGN) postulates the existence of a thick molecular/dusty torus surrounding a black-hole/accretion-disc system (see, e.g. Krolik 1999). Attempts to unveil this torus in a nearby AGN like NGC 1068 have drawn considerable effort on the side of high spatial resolution imaging, in particular in the near-IR (Chelli et al. 1987, Gallais, 1991, Young et al. 1996, Marco et al. 1997, Thatte et al. 1997, Rouan et al. 1998, Alloin et al. 1999, Wittkowski et al. 1998, Weinberger et al. 1999, Marco & Alloin, 2000) and mid-IR (Braatz et al. 1993, Cameron et al. 1993, Bock et al. 1998, Lumsden et al. 1999). With respect to the presence of such a torus, the most compelling results are: (a) VLBA 8 GHz data (Gallimore et al. 1997) revealing a 1 pc elongated distribution of ionized gas at PA $\approx$ 110° (the inner "hot zone" of the torus?), (b) adaptive optics (AO) observations at 2.2 μm (Rouan et al. 1998) showing extended emission along PA $=$ 102° and up to a 15 pc radius (in addition to a prominent unresolved core with size less that 9 pc and in addition to another 20 pc radius extended emission along PA $=$ 15° which follows the Narrow Line Region) and at 3.5 and 4.8 μm (Marco & Alloin, 2000) revealing structures similar in shape/orientation and on comparable scales, (c) near- and mid-IR imaging polarimetry (Lumsden et al. 1999) calling for the presence of hot and warm dust components fully consistent with those detected with AO. The structure elongated at PA $\approx$ 102° could trace the equatorial plane of an inclined dusty/molecular torus, from its inner walls of ionized material seen in radio, to its outer parts of thermally emitting dust with a temperature range from T $\approx$ 1500 K (dust sublimation temperature) to a few 100 K.

Models by Krolik & Begelman (1986), Pier & Krolik (1993), Efstathiou & Rowan-Robinson (1994), Granato & Danese (1994), and Granato et al. (1997) have explored torus sizes from 1 to 100 pc. They predict emission in the near-IR and mid-IR and provide high resolution model-maps at various wavelengths. Therefore, it is particularly timely to obtain high resolution mid-IR images to compare with model-maps.

Here, we present and discuss new results from diffraction-limited images obtained with the CFHT/Hawaii and ESO/La

Silla 3.6m telescopes, at 11.2 and 20.5 μm respectively. Hereafter, the distance used for NGC1068 is 14.4 Mpc, leading to the equivalence $1'' \approx 70$ pc in the object.

2. Data collection and reduction

The observations were performed using the CEA/SAp mid-IR camera CAMIRAS (Lagage et al. 1993), equipped with a Boeing 128x128 pixels BIB detector which is sensitive up to 28 μm. The AGN in NGC1068 was observed with CAMIRAS attached to the ESO/La Silla 3.6m telescope on 1998 November 8–10 and to the CFHT/Hawaii 3.6m telescope on 1999 August 1. During these two runs seeing and weather conditions – humidity and amount of atmospheric precipitable water – were particularly favorable to observing in the mid-IR and extremely stable.

The orientation of the array on the sky was carefully determined at the start of each observing run. The pixel size was $0.315''$ (20 μm window, ESO/La Silla) and $0.29''$ (11 μm window, CFHT/Hawaii).

In the 20 μm window, we used a filter centered at 20.5 μm and with a bandpass (FWHM) $\Delta\lambda$ = 1.11 μm. This filter is free of any important line contribution. In the 11 μm window, we used a filter centered at 11.2 μm and with a bandpass $\Delta\lambda$ = 0.44 μm: although the 11.3 μm PaH line emission falls within this filter, one should notice that the spectroscopic results from the ISO satellite do not show its presence in the AGN of NGC 1068 (aperture of $3''$). Therefore we are confident that these two filters reflect mostly the mid-IR continuum emission of the AGN. To avoid saturation of the detector by the high ambient photon background, the image elementary integration times were chosen to be 9.1 msec and 19.1 msec, respectively at 20.5 and 11.2 μm. Standard chopping and nodding techniques were applied with a chopping throw of $20''$. Elementary images were coadded in real time during 3 sec chopping cycles. At 20.5 μm a total integration time of 22.5 min was spent on the source observed at an airmass less than 1.3. At 11.2 μm, the total integration on source was of 65 min and the mean airmass of 1.04. A shift-and-add procedure was applied to the final images through each filter. The final signal-to-noise ratio at the peak emission on the images is 265 at 20.5 μm and 980 at 11.2 μm.

The nearby reference star τ 4 Eri was frequently monitored to serve as a PSF and flux standard at 20.5 μm, while α Ceti was used at 11.2 μm (van der Bliek et al. 1996). The precision achieved in flux measurements is +/– 5% and +/– 10%, respectively at 11.2 μm and 20.5 μm.

Because final images are limited by the seeing and above all by the 3.6m telescope diffraction-pattern (FWHM of $1.4''$ and $0.8''$ at 20.5 μm and 11.2 μm respectively), applying a deconvolution procedure is mandatory. We use the Entropy Method developed by Pantin & Starck (1996), based upon wavelet decomposition. The Shannon theorem (1948) prescription allows to persue the deconvolution down to twice the pixel size, in this case down to $0.6''$, and iterations are stopped according to the residual map, whose properties should be consistent with data noise characteristics.

3. Results and discussion

3.1. Structure and flux contributions

We provide in Fig. 1 a set of the images at 20.5 μm: the NGC1068 image before deconvolution, the PSF stellar image, and the NGC1068 image after deconvolution. A similar set of images at 11.2 μm is displayed in Fig. 2. The general orientation of the extended emission runs through the North-East to South-West quadrants, with a noticeable North-South elongation of the inner isophotes. The deconvolved image and contours at 11.2 μm are fully consistent with the map at 12.4 μm obtained at a comparable spatial resolution by Braatz et al. (1993). In the 10 μm window, the speckle data (over a $5'' \times 5''$ region, with a resolution down to $0.2''$, but with a smaller dynamical range) analyzed by Bock et al. (1998) indicate however a different orientation with the extended emission in the inner $5'' \times 5''$ region running through the North-West to South-East quadrants: this does not appear to be consistent with either Braatz et al. (1993) or the new data set presented in this paper. This discrepancy remains to be elucidated.

The deconvolved images, both at 11.2 and 20.5 μm show the presence of a prominent central core. Cuts through the core along the North-South and East-West directions provide FWHM values of $0.9''$ and $0.6''$ respectively. Therefore, the core remains unresolved in the East-West direction, while it appears to be extended North-South with intrinsic FWHM size of around 50 pc. Again this result is in very good agreement with Braatz et al. (1993).

Regarding the extended emission, one notices that conspicuous features can be seen further away from the core at 20.5 μm than at 11.2 μm. In the North-East quadrant we have identified two clouds, (a) and (b), along PA $= 35°$, at mean distances from the core of $3.7''$ and $1.8''$, respectively. Cloud (a), which is bright both at 11.2 and 20.5 μm, appears to widen perpendicularly to the main direction of the extended emission and runs from PA $= 15°$ to PA $= 55°$. In the South-West quadrant, the emission closest to the core extends along PA $= 210°$ and then aligns North-South: two clouds, (c) and (d), can be singled out at mean distances from the core of $2''$ and $3.5''$. The results are summarized in Table 1.

Flux measurements at 11.2 and 20.5 μm have been performed using a mask built from the 20.5 μm image and delineating the extent of the four clouds and of the core, so that the 11.2 μm to 20.5 μm flux ratio can be derived in a consistent fashion. The mask at the position of the core takes into account the full extent ($2'' \times 1.2''$) of the core (rather than its FWHMs values given in Table 1). The resultant fluxes are given in Table 1: one notices that the core contributes a very large fraction of the mid-IR emission, 95.6% at 11.2 μm and 94% at 20.5 μm.

3.2. Comparison with maps at other wavelengths

We have just seen that the mid-IR emission extends away from the core up to a radius of about 300 pc, both in the North-East and South-West quadrants. In order to compare this extension/structure to those observed at other wavelengths, in the

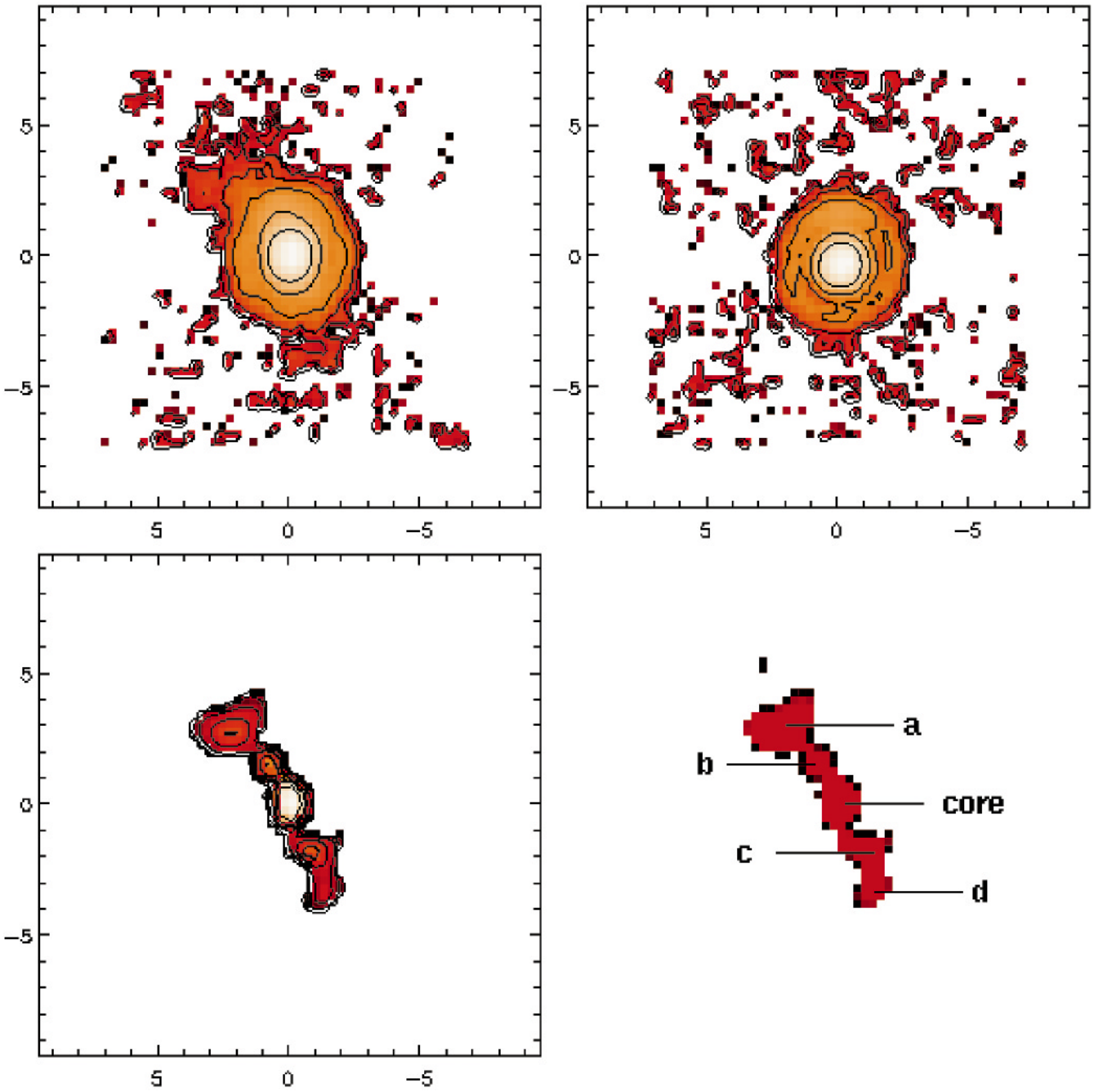

Fig. 1. The 20.5 μm data. Top left: the NGC 1068 raw image. Top right: the reference star used as PSF. Bottom left: the deconvolved image of NGC 1068. The bottom right image shows a sketch of the 5 structures discussed in the text, clouds (a),(b),(c),(d) and the core. On all images, North is to the top, East to the left. The pixel scale is $0.315''$/pixel, and the total field spans about $19.2'' \times 19.2''$. On the raw image and the PSF image, a series of 6 contours (step by factor 3 in intensity from one to the next) has been superimposed. On the deconvolved image, 8 contours (same step) have been superimposed.

radio range with the VLA or in the UV/optical with HST, it is mandatory to register precisely the mid-IR map with respect to the near-IR, visible and radio ones.

As we did not have the possibility to perform astrometric measurements through simultaneous observations in the mid-IR and near-IR or visible (as performed in Marco et al. 1997), we are assuming firstly that the cores at 11.2 and 20.5 μm are coincident and secondly that their location also coincides with that of the cores observed at 4.8, 3.5 and 2.2 μm. Regarding the first assumption, one can check from the model of NGC 1068 developed by Granato et al. (1997) which predicts the offsets between emission peaks at various wavelengths in the near-IR to mid-IR, that these offsets remain in the range of a few hundredths of an arc second and can be ignored. Regarding the

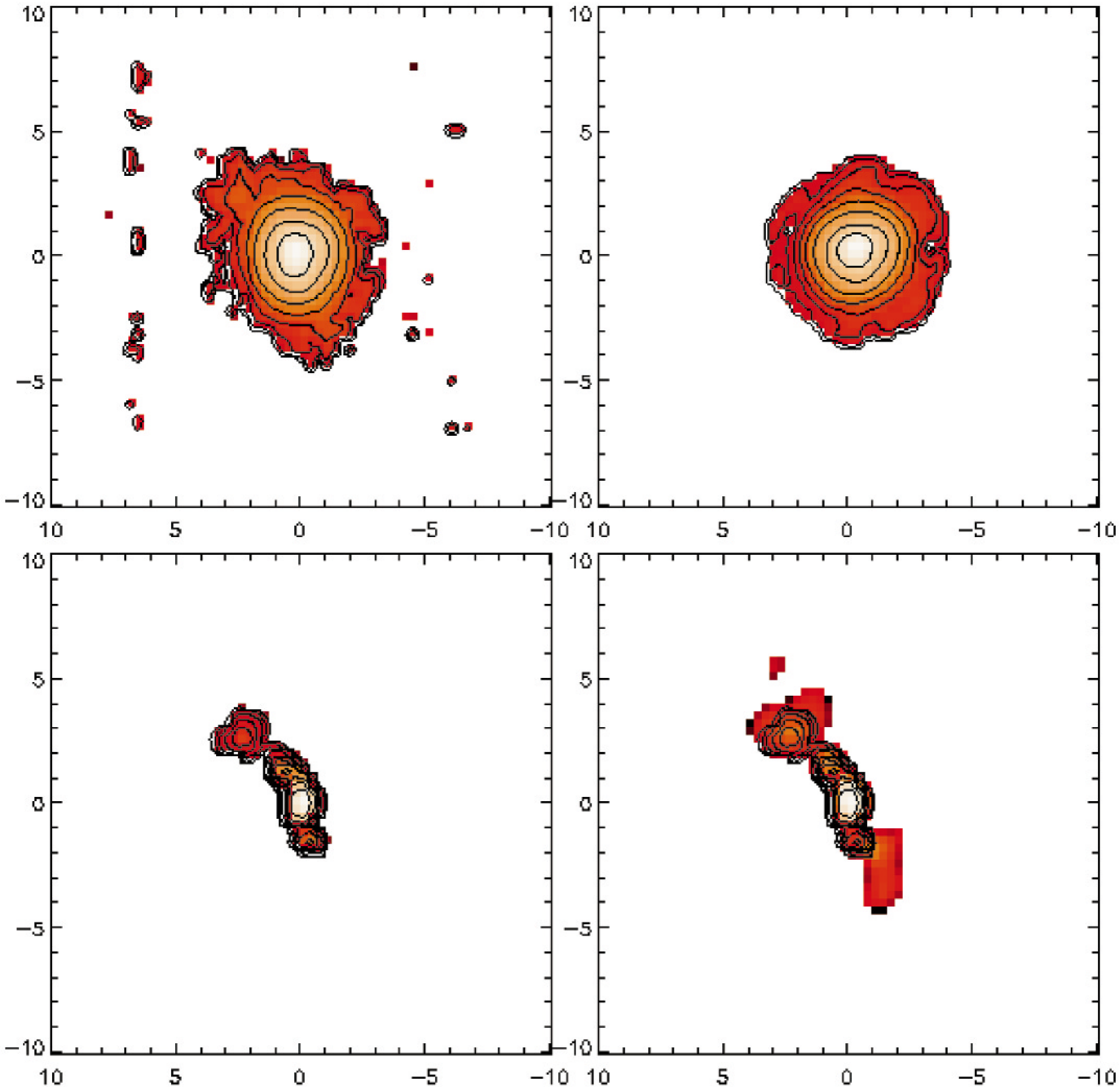

Fig. 2. The 11.2 μm data. Top left: the NGC 1068 raw image. Top right: the reference star used as PSF. Bottom left: the deconvolved image of NGC 1068. On all images, North is to the top, East to the left. The pixel scale is $0.29''$/pixel, and the total field spans $20'' \times 20''$. On the raw image and the PSF image, a series of 8 contours (step by factor 3 in intensity from one to the next) has been superimposed. On the deconvolved image, 10 contours (same step) have been superimposed. The bottom right panel features in its background the 20.5 μm deconvolved image on top of which the 11.2 μm contours have been superimposed, showing the correspondence of structures at 11.2 and 20.5 μm. Note that cloud (d) seen on the 20.5 μm image is not detected at 11.2 μm, probably because of temperature and opacity effects.

second assumption, the cores observed at 4.8, 3.5 and 2.2 μm have been shown to be positionally coincident indeed (Rouan et al. 1998, Marco & Alloin 2000). And finally, Marco et al. (1997) have obtained the astrometric positioning of the core at 2.2 μm, with respect to the HST map in the visible of the central area in NGC 1068: it was found to be located $0.28''$ South and $0.08''$ West of the so-called optical continuum peak seen with HST (Lynds et al. 1991). The study by Marco et al. (1997) also allowed a precise registration of the 2.2 μm map with respect to the 12.4 μm map from Braatz et al. (1993) and to available radio, optical and UV maps. The conclusion is that the core at 4.8, 3.5 and 2.2 μm appears to be coincident with the

Table 1. Position, size and flux measurements of the various structures identified at 20.5 μm, as derived from the deconvolved image (down to a final resolution of $0.6''$). The extension provided for the core corresponds to the FWHMs of its E-W and N-S profiles, while the extension quoted for the clouds (a), (b), (c) and (d) corresponds to a full size as measured from the map at 20.5 μm. Fluxes given in this table have been obtained through a mask fitting the full extent of the core and of each of the clouds (see text). The total flux found at 11.2 μm in 1999 is about 30% larger than the figure quoted by Lumsden et al. for the year 1995. According to Glass (1997) and Marco & Alloin (2000), the 3.5 μm flux has been increasing steadily since 1974. Therefore, the 11.2 μm flux difference found between 1995 and 1999 is most probably related to an intrinsic flux increase of the AGN.

Component	Extension ($''\times''$)	Distance ($''$)	Flux 20.5 μm (1σ error, (Jy))	Flux 11.2 μm (1σ error,(Jy))
Core	0.6×0.9	0	57.5 (6)	37.5 (2)
(a) N-E	1.8×4.0	3.7	1.4 (0.1)	0.15 (0.01)
(b) N-E	1.3×1.3	1.8	1.1 (0.1)	2.6 (0.15)
(c) S-W	1.3×1.6	2.1	1.0 (0.1)	0.3 (0.02)
(d) S-W	1.3×1.3	3.5	0.15(0.01)	undetected

12.4 μm peak position found by Braatz et al., the radio source S1, the symmetry center of polarization both in the UV/optical (Capetti et al. 1995) and in the mid-IR (Lumsden et al. 1999). We consider this core to feature the central engine (hidden in UV/optical maps) and from all the above quoted studies we can ascertain the consistency of the assumptions made earlier.

We have compared the mid-IR maps at 11.2 and 20.5 μm to the radio maps and to the HST [OIII]–emitting cloud map, provided on a suitable scale in Bland-Hawthorn et al. (1997) and with a registration as above. We have reached the following conclusions:

– compared to the radio maps from Gallimore et al. (1996a,b) and Muxlow et al. (1996), the observed North-South elongation of the mid-IR core is reminiscent of the North-South alignment of the radio sources S2, S1 and C (see Fig. 2 in Bland–Hawthorn et al. 1997 for a synthesis of the radio source nomenclature after Wilson & Ulvestad 1987). At the location of radio source C, the orientation of the radio jet-like structure changes abruptly and becomes close to PA $= 35°$, matching then the general direction of the mid-IR extended emission in the North-East quadrant. The mid-IR cloud (a) coincides perfectly with the wide base of the so-called Northeast radio lobe. In the South-West quadrant, the radio jet-like structure is along PA $= 210°$ again very well aligned with the mid-IR extended emission. The so-called Southwest radio hotspot is situated about $4''$ away from the central engine, S1, and can be put in correspondence with the mid-IR cloud (d).
– compared with the HST [OIII]–emitting cloud map, the North-South elongation of the mid-IR core is found to overlap to the North with HST cloud-A and cloud-B, two NLR clouds distributed along the North-South direction. The extended mid-IR emission in the North-East quadrant is along PA $= 35°$ and arises to the eastern edge of the ionizing cone (which, on a large scale extends between PA $= -15°$ and PA $= 35°$) defined by the [OIII]–emitting complexes, beyond cloud-F and to the East of cloud-G which is itself located about $2''$ away from the central engine. It should be noted as well that the mid-IR cloud (a) is located very close to an optical emission knot early identified in the literature as the "Northeast knot" in the direction PA $= 35°$ and at a distance about $4''$ from the central engine (Elvius 1978 for the first identification). The extended mid-IR emission in the South-West quadrant has no counterpart in the HST [OIII]–emitting cloud map, as expected from the heavy obscuration on that side of the AGN. Therefore, it is conspicuous that the extended mid-IR emission in the North-East quadrant arises aside the NLR (as featured by the [OIII]–emitting clouds) and from material which is not directly exposed to the central ionizing source. However, the tight correlation existing between the mid-IR extended emission and the 4.9 GHz emission is a result which signals the importance of the radio jet-like emission impacting on interstellar material located above and below the equatorial plane of the dusty/molecular torus.

3.3. Nature of the mid-IR core

The emission core observed at 11.2 and 20.5 μm shows a noticeable North-South extension, about 100 pc, while it remains unresolved (< 50 pc) along the East-West direction. In the model devised by Granato et al. (1997) of the AGN in NGC 1068, a 100 pc torus and a viewing angle of 65° were the torus parameters finally selected to match the SED of the AGN. This model predicts indeed that maps of the torus emission in the mid-IR should be elongated perpendicularly to the torus plane, in this case roughly along the North-South direction, and on a scale of +/– $0.5''$. One should notice however that the model maps have been obtained after convolution with a PSF FWHM $= 0.09''$, too narrow compared with the effective PSF of the data presented in this paper. Yet, the predicted direction of the elongation is consistent with the observed one at 11.2 and 20.5 μm and its predicted size has the right order of magnitude, if compared to the measured one.

Comparing the core at 11.2 and 20.5 μm to high resolution maps at 4.8, 3.5 and 2.2 μm (Marco & Alloin 2000, Rouan et al. 1998) is more difficult because of the difference in spatial resolution. Indeed, the extensions (both polar and equatorial) seen at 4.8, 3.5 and 2.2 μm are entirely enclosed within the 11.2 and 20.5 μm core size. Yet, if the PA $= 102$ ° equatorial extension detected at 4.8, 3.5 and 2.2 μm features the torus itself, one might expect to see emission in the mid-IR from cool dust located further away than the warm dust emitting at 4.8 μm, still along (PA $= 102°$). Such emission is not detected. One possible interpretation is that the equatorial extension at 4.8, 3.5 and 2.2 μm does not directly feature the torus. This indeed would be surprising, because the covering factor of the equatorial extension to the central source is smaller than expected on the basis of several arguments (opening angle of the ionizing cone, ratio between IR and primary UV radiation...). The extended equatorial emission at 4.8, 3.5 and 2.2 μm could instead trace

only the equatorial plane of the torus rather than the torus itself (possibly smaller) and outline the merging of the torus with the host–galaxy disc, in regions of high density where star formation is occurring and provides an additional and local source of heating. This would explain the presence of dust at a temperature much higher than that predicted by torus models which take only into account the heating from the central engine. The dust emission in these regions located in the torus equatorial plane but "around-the-torus" could then be more prominent at 4.8 than at 11.2 and 20.5 μm. In fact there is a whole new area to be explored at the transition between the molecular/dusty torus and its environment.

3.4. Origin of the extended structure

The comparison of maps in the radio, mid-IR, near-IR and optical/UV can potentially bring clues about the origin of the mid-IR extended emission beyond the torus itself: extra dust components, location, source of heating, etc. Unfortunately, one cannot yet confront in detail the observed maps with predicted model-maps for the following reason: existing AGN models are targeted at representing the molecular/dusty torus itself rather than the full molecular/dusty environment of an AGN and therefore do not take into account the presence of the NLR region or more generally the distribution of matter away from the torus itself. For example, thermal emission from warm dust possibly surviving on the back and UV–protected side of NLR clouds is not considered, the impact of the radio jets on intervening material such as the NLR clouds or massive molecular clouds away from the equatorial plane of the torus are not taken into account either.

On the contrary, current results on the extended mid-IR emission in NGC 1068 are telling us that material is present and heated around and away from the torus itself, up to a distance of $\approx$ 300 pc. Assuming silicate grains with a power–law (-3.5 exponent) size distribution over the size range 0.01 to 0.1 μm, the 11.2 to 20.5 μm flux ratio observed in cloud (a) and cloud (c) implies temperatures of around 150 K. Cloud (a) is already more than 200 pc away from the central engine and on the edge of the ionizing cone: how are the grains heated up to this temperature? What is the role played by single photon transient heating of small grains? by the radio jet-like structure which appears to coincide so closely with the mid-IR extended emission? These questions deserve a more complete analysis and a quantitative modeling which is deferred to a specific and later work.

3.5. Concluding remarks

Mid-IR imaging at high angular resolution offers potential advantages in the study of AGN environment because this wavelength range is specific of warm/cool dust emission (and possibly synchrotron emission from electrons) and because extinction is reduced. The diffraction-limited images (resolution ($0.6''$)) presented in this work highlight the presence of a prominent core emitting about 95% of the total flux in the mid-IR, as well as of extended emission, up to $4''$ to the South-West (PA = 210°) and $4''$ to the North-East (PA = 35°), broken into patchy components which are particularly conspicuous at 20.5 μm and can be singled-out as individual clouds. The central core shows an unresolved East-West FWHM of $0.6''$ and a North-South FWHM of $0.9''$ corresponding to a resolved full size extension of $\approx$ 100 pc. The North-South elongation of the emission core agrees with predicted maps of the mid-IR emission from a 100 pc dusty/molecular torus surrounding the central engine in NGC 1068 and observed under an inclination angle of around 65°. As a result of smaller optical depth, the extended emission in the North-East and South-West quadrants is more prominent at 20.5 than at 11.2 μm. The extended emission follows roughly the direction of the radio-jet and radio-lobe structures. In the North-East quadrant, the mid-IR emission is located at the eastern edge of the ionizing cone outlined by the HST [OIII]– emitting clouds. Interpreting the complete molecular/dusty environment of the AGN, both in the torus and away from it, pleas for the development of three-dimensional complex modeling. High resolution imaging is the first step in disentangling the various components: the new generation of 8m–10m class telescopes provides a resolution of $0.3''$ in the mid-IR. Subsequent integral-field spectroscopy with such a spatial resolution and interferometry will also constitute invaluable tools to resolve this type of problem.

Acknowledgements. We are gratefully indebted to R.Jouan and M.Lortholary for their efficient assistance with the CAMIRAS instrument, as well as to the staff at both ESO/La Silla and CFHT/Hawaii for their support during the observing runs. We acknowledge careful comments from the referee R.Antonucci.

References

Alloin D., Clenet Y., Granato J.L., et al., 1999, In: Bonaccini D. (ed.) Astrophysical Results from Adapative Optics. ESO Conference and Workshop Proceedings 56, p. 21
van der Blieck M., Manfroid J., Bouchet P., 1996, A&AS 119, 547
Bland–Hawthorn J., Gallimore J., Tacconi L., et al., 1997, Ap&SS 248, 9
Bock J., Marsh K., Ressler M., et al., 1998, ApJ 504, L5
Braatz J.A., Wilson A.S., Gezari D.Y., et al., 1993, ApJ 409, L5
Cameron M., Storey J.W.V., Rotaciuc V., et al., 1993, ApJ 419, 136
Capetti A., Maccheto F.D. Axon D.J., et al., 1995, ApJ 452, L87
Chelli A., Perrier C., Cruz-Gonzales I., et al., 1987, A&A 177, 51
Efstathiou A., Rowan-Robinson M., 1994, MNRAS 212, 218
Elvius A., 1978, A&A 65, 233
Gallais P., 1991, Ph.D. Thesis, Université Paris 7
Gallimore J.F., Baum S.A., O'Dea C.P., et al., 1996a, ApJ 458, 136
Gallimore J.F., Baum, S.A., O'Dea C.P., et al., 1996b, ApJ 462, 740
Gallimore J.F., Baum, S.A., O'Dea C.P., 1997, Nat 388, 852
Glass I., 1997, Ap&SS 248, 191
Granato G.L., Danese L., 1994, MNRAS 268, 235
Granato G.L., Danese L., Franceschini A., 1997, ApJ 486, 147
Krolik J.H., 1999, In: Active Galactic Nuclei. Princeton University Press
Krolik J.H., Begelman M.C., 1986, ApJ 308, L55
Lagage P.O., Jouan R., Masse P., et al., 1993, SPIE 1946, 655
Lumsden S., Moore T., Smith C., et al., 1999, MNRAS 303, 209

Lynds R., Faber S.M., Groth E.J., et al., 1991, ApJ 369, L31
Marco O., Alloin D., Beuzit J.L., 1997, A&A 320, 399
Marco O., Alloin D., 2000, A&A 353, 465
Muxlow T.W., Pedlar A., Holloway A., et al., 1996, MNRAS 278, 854
Pantin E., Starck J.-L., 1996, A&AS 118, 575
Pier E.A., Krolik J.H., 1993, ApJ 418, 673
Rouan D., Rigaut F., Alloin D., et al., 1998, A&A 339, 687
Shannon C., 1948, Bell Systems Technical Journal 27, 379 & 623
Thatte N., Quirrenbach A., Genzel R., et al., 1997, ApJ 490, 238
CFHT
Wilson A.S., Ulvestad J.S., 1987, ApJ 319, 105
Weinberger A., Neugebauer G., Matthews K., 1999, AJ 117, 2748
Wittkowski M., Balega Y., Beckert T., et al., 1998, A&A 329, L45
Young S., Packham C., Hough J.H., et al., 1996, MNRAS 283, L1